CAMBRIDGE
UNIVERSITY PRESS

RESEARCH ARTICLE

Design and position control of a robotic brace dedicated to the treatment of scoliosis

Rahul Ray[1,2,*] , Laurence Nouaille[1], Briac Colobert[2], Laurine Calistri[2] and Gérard Poisson[1]

[1]PRISME Laboratory, University of Orléans, Orléans, France and [2]Department of Research and Development, Proteor Company, Dijon, France
*Corresponding author. E-mail: rahul.ray@etu.univ-orleans.fr

Abstract
This paper's content focuses on designing and prototyping a robotic brace dedicated to treating scoliosis. Scoliosis is an abnormal spinal curvature affecting 1–3% of children and constitutes a major therapeutic problem. In moderate cases of deformity, passive brace treatment is performed. However, this approach can lead to important patient discomfort. So, we propose a robotic solution providing greater mobility and the possibility of adapting the procedure to each patient. The robotic brace we built and tested is composed of three specific rings adapted to the patient's torso. Each independent module of two consecutive rings is movable through a Stewart–Gough platform-type mechanism. As the robotic brace is lightweight, it brings better portability and improves the patient's comfort.

The first part of the paper shows the state of the art of bracing techniques: from passive to active orthoses. Next, the mechatronics of the device is detailed, and the robot's kinematic models are developed. The motion control principle is given. In the last part, motion tests were administered with a healthy human to validate the brace architecture choice and its position and motion control strategies.

1. Introduction

1.1. From spinal deformity to bracing

Scoliosis is among the most complex and common spinal deformities characterized by a three-dimensional deformation of the spine [1, 2]. In general, 50–80% of adolescents with scoliosis (1–3% of children being affected) have idiopathic scoliosis, the most usual form with unknown etiology [3, 4], and 30,000 children worldwide are prescribed braces to treat scoliosis. At the same time, 38,000 patients undergo spinal surgery annually [2, 5]. About 0.3–0.5% of population need scoliosis treatment [6]. As can be seen in an X-ray image of the spine of a person with scoliosis, the curve of the spine is more like a "C" or an "S" than a straight line, see Fig. 1 [7]. The Cobb angle, see Fig. 1, is a parameter conventionally used by experts to evaluate this curvature [1, 2]. It is measured in the coronal plane using standard posteroanterior radiographs [8]. A Cobb angle of 10 degrees or more added to proof of evolution leads to a diagnosis of scoliosis needing to be treated [9]. Observation and bracing are the two non-operative treatments for scoliosis, which can reduce the costs of therapy. Several researches have shown that brace treatments are more effective than observation [10, 11]. This disorder usually appears during the adolescent years of growth and progresses until skeletal maturity. Such abnormal curves can make the individual's shoulders or waist appear uneven, Fig. 1. The bones are also rotated, making one shoulder blade more prominent than the other [7]. Scoliosis may also impact the quality of life of those affected by limiting their daily activities, causing pain, reducing respiratory function, and diminishing self-esteem [2]. Severe scoliosis (when the Cobb angle is greater than 40°) is commonly associated with
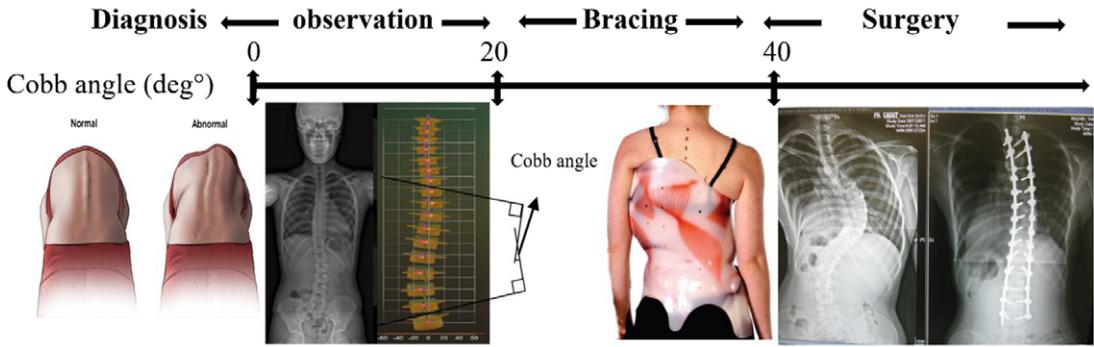
Figure 1. *Treatment options depend on the Cobb angle. Source: online resources from Smartist software ©Proteor.*
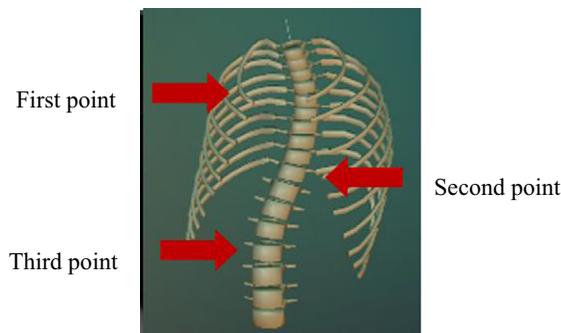
Figure 2. *Three-point pressure technique is applied to the spine (Adolescent idiopathic scoliosis type C). Source: Smartist software ©Proteor.*

the body's restricted digestive, hormonal, musculoskeletal, and neurological function [8]. Spinal fusion is highly recommended in such cases [6, 12]. In response to this basic need for scoliosis treatment, the most classic non-invasive technique is bracing, see Fig. 1. Our work focuses on this approach with deep collaboration with Certified Prosthesis and Orthosis experts from Proteor enterprise. The brace described in this article applies forces and moments to the body at specific spine areas through position control mode.

1.2. Bracing techniques for treatment of scoliosis
1.2.1. The standard "three-point pressure" for the treatment of scoliosis
The most appropriate treatment for adolescent idiopathic scoliosis is bracing using the "three-point pressure" technique. Depending on the type of scoliosis, this technique is exerted on the abnormal curvature of the human spine to contain the natural progression of the spine. Through this practice, different pressures are exerted on three distinct zones on the convex part of the spine to hold the spinal cord in a straighter posture, see Fig. 2.

1.2.2. Passive bracing
A scoliosis brace is typically a rigid plastic framework that matches the spine and hips and applies pressure on the abnormal curvature of the spine [13, 14]. A passive brace is sometimes recommended to be worn for up to 16–18 h daily to restore a deformed spine position/curve to a correct posture [15, 16].
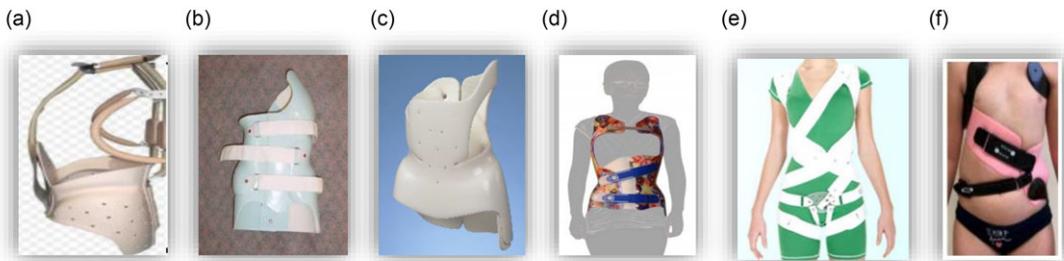
Figure 3. *Several types of scoliosis brace: (a) Milwaukee* [20], *(b) Charleston* [21], *(c) Boston* [17], *(d) Cheneau* [18], *(e) Spinecor, (f) 3D Spirale brace. Source: online resources and figure (d) and (f) from* © *Proteor.*

Based on the scoliosis type, there are different shapes of braces with multiple functions and performances [17–20], as shown in Fig. 3(a)–(f). Passive braces are all composed of either one rigid body or multiple bodies rigidly connected.

The Milwaukee brace, Fig. 3(a), [7, 20, 22] applies traction to the spine through a steel and leather pelvic base supporting the brace, vertebral bars, and a neck ring. Although patients must extend their spine to escape the occipital-mandibular assemble, it uses the self-correction principle.

The Charleston bending brace, Fig. 3(b), is employed primarily during nighttime to manage compliance issues in patients with scoliosis for whom other treatment options had failed [17, 20–22].

The Charleston bending brace was designed to biomechanically correct abnormal posture of the spine by stabilizing, lateral shift, and traditional bracing methods to apply unbending forces based on three-point pressure systems [19].

The Boston brace, Fig. 3(c), is quite effective and complies with passive bracing for scoliosis [23–26]. This brace consists of a fabricated plastic piece with diverse sizes of paddings to correct deformities within the lumbar, thoracolumbar, and thoracic regions of the spine. It applies three-point pressure with rotation [19].

The Cheneau brace, Fig. 3(d), consists of multiple rigid parts that help provide the necessary care to the upright structure of the spine to correct abnormal posture. Three-point pressure is the principle of the bracing technique that pushes the abnormal curve inwards while being passive at the two ends of the brace [18].

As traditional bracing techniques have evolved toward an emphasis on mobility and design, the SpineCor brace, Fig. 3(e), was proposed, which uses a series of elastic straps [27] to correct the curvature of the spine [28]. The 3D spiral brace is a semi-rigid passive brace which shows that research on material and design is ongoing with passive braces, Fig. 3(f).

1.2.3. Active bracing

The role of an active brace is also to correct the abnormal posture of the spine. As a passive brace is rigid and typically restricts normal activities of daily life, it might be uncomfortable, making it difficult to wear for extended periods and resulting in poor user compliance [7, 28, 29]. Therefore, Lou et al. proposed an active bracing approach. They created a pneumatic device capable of increasing or decreasing the pressure from a pad internal to the brace to attain proper brace tension [30]. Other active braces are implemented with actuators to apply corrective force, Fig. 4(a) [31] and Fig. 4(b) [32]. These designs are active in modulating the forces/torques in three-dimensional movement [32] but still lack the effectiveness of the treatment, limiting their application in medical practice.
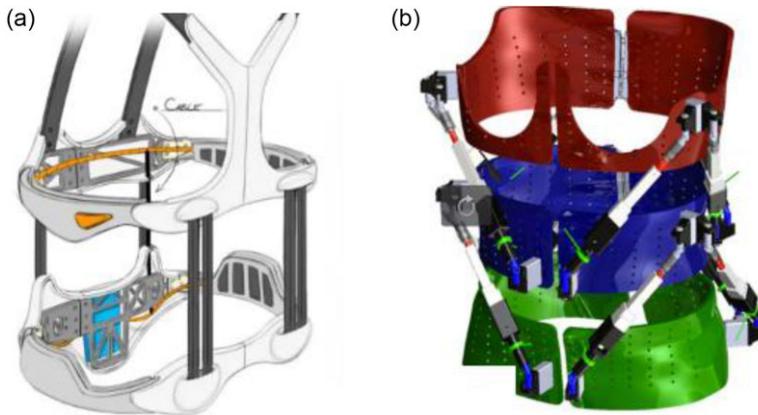
Figure 4. *(a) ExMS-1brace from ExoDynamics* [31], *(b) Rose brace from roar lab* [32]. *Source: online resources.*

1.2.4. Discussion

Several constraints are still lacking in the current bracing techniques that include the following:

- Braces cannot realize precise control over the spine.
- They cannot apply pressure over the specific area of the spine as it only applies to the muscles.
- They can cause muscle weakness by being in the brace for 18–20 h daily.
- The brace is not modulated based on the user's needs.
- Braces limit daily life activities, including eating, sitting, standing, and other sporting activities.
- These bracing methods cause pain, muscle breakdown, and abnormal deformation of bone.
- Their bulky designs are unlikely to be adopted by the patients because of the wearer's discomfort.
- There is a lack of user interface between the wearer and the brace for modulating the position control for better motion and mobility.

Based on this reasoning [7], the robotic can address the following constraints in limitations of the bracing technique:

- manage the restrictions in current brace designs,
- add actuated components and sensors to modulate the brace properties during usage,
- provide monitoring of the position of the brace remotely with built-in position sensors,
- exert corrective three-point pressure on the spine in three dimensions,
- lighten the device with a comfortable material for patient comfort,
- use command-line interface between the brace and the wearer,
- control the brace position with a compact real-time interface.

To effectively treat scoliosis and allow better mobility and displacement than a passive brace, an active brace requires the exertion of a continuous three-point pressure on the spine. We designed our robotic brace on the biomechanical principles of orthotics and the three-point pressure theory. Lightweight decreases the risk of discomfort for the patients and permits more effortless motion during daily activities. In addition, it can modulate mobility based on the user's needs. First, we present the mechanical brace design and its kinematic analysis in Sections 2 and 3 – next, the position control of the brace in Section 5 – finally, experimental evaluations of the position control of the brace feature in Section 6.
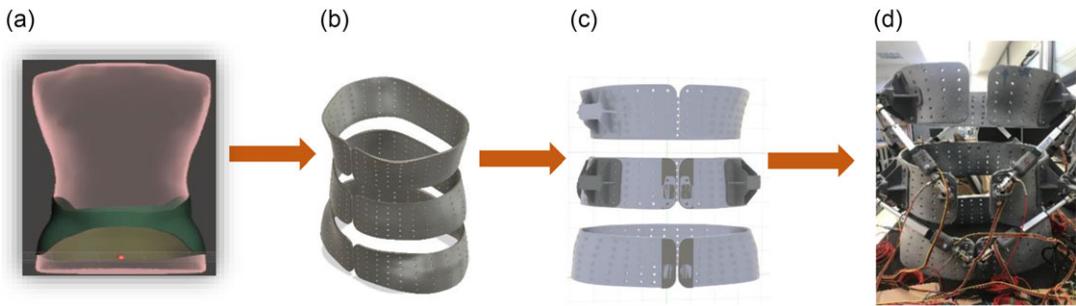
Figure 5. *Outline of brace concept: (a) 3D scan of the body; (b) 3D-printed three rings; (c) Rings assembled with mounting parts; (d) Fully assembled robotics brace.*

2. Design method for the robotic brace

2.1. Mechanical structure of robotic brace

Concerning the three-point pressure technique, the designed prototype of a robotic brace fits specially to a volunteer. The designed brace consists of three articulated rings that may be adjusted to fit the human body better. They are held on the trunk's pelvic, mid-thoracic, and upper thoracic regions, Fig. 5(b). The pelvic ring is tightly fixed to the pelvis, so it is considered immobile regarding the pelvic reference frame. The mid-thoracic ring can move relative to the pelvic ring in a six-degrees-of-freedom (DOF) motion.

In the same way, the upper ring can move relative to the mid-thoracic ring in a 6 DOF motion. It provided each relative mobility by combining six linear actuators arranged between two consecutive rings like a Stewart–Gough platform. Therefore, it is twelve actuators integrated into the device. Rings are patient-specific, so we have implemented a particular procedure to design and manufacture them. The three rings exert forces on the patient's body based on the three-point pressure bracing technique: Optical scanning got a 3D scan of the body, Fig. 5(a). Next, we make a 3D CAD model of the scan body shape using the 3D scan data. Then, this model superimposed the 3D CAD model of the spine to get the spine model's approximate location of the spine vertebrae. Next, the areas and sizes of the three rings are determined. Finally, we designed a brace ring using rigid 3D-printed material, Fig. 5(b).

Before integrating the accurate actuators, we developed a complete model of the device (including printed actuators and sensors). Then, we have additive fabrication to have a precise understanding of the overall volume of this device and its mobilities, thus having a reasonable expectancy of patient comfort when fitted with our brace, Fig. 5(c).

2.2. The various components of the device

To drive the two Stewart–Gough platforms, this brace is equipped with twelve linear electric actuators. The joints between each actuator and each ring are universal joints (U) disposed at the base and the top of the actuators. The sliding link is the one that is actuated (P) So, each actuator constitutes a leg for the parallel mechanism, giving the robot a 6UPU structure.

Moreover, the actuators have an attached load cell at the base for measuring the actuated force/torque driven through a conditioning board to control the input and output voltage for each actuated parallel platform of the brace. A motor driver is used for the Pulse Width Modulation control (PWM) of each linear actuator which has a built-in potentiometer. All the control modules of the brace are driven through a real-time controller. The various elements of the brace are explained below.
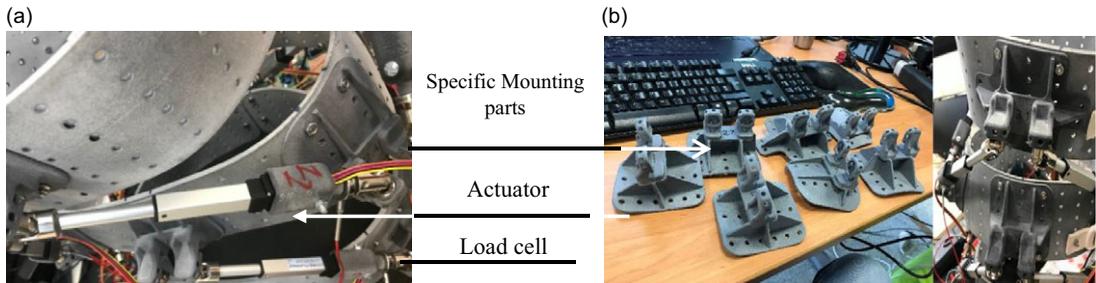
Figure 6. *(a) Robotic brace with actuator and load cell; (b) Mounting parts.*

2.2.1. The linear electric actuators

The linear actuators integrated with this robotic brace are from Actuonix Company with a gear ratio of 210:1 and operate at 12 V (a higher gear ratio leads to applying higher force by the robotic brace on the spine). They provide 5 cm of stroke length; see Fig. 6(a). They are capable of a peak force of 45 N and a peak speed of 5 mm/s allowing a peak power point of 62 N with a rate of 3.2 mm/s (allows consistent control of brace movement). They have high flexibility and make up a configurable and compact platform for the smooth mobility of the robotic brace. The linear actuators have a built-in potentiometer that provides a position feedback signal that can be input to the robotic brace controller to modulate brace mobility. Although they have an optional onboard microcontroller, we developed an external control device and drove the actuator at high frequency. We describe explicit expressions for the movement of the actuators in mechanical design parts. A similar approach and mathematical formulations are in [33–35].

A series of holes have been built in the three rings to place the actuators in the best configuration on the brace and to respect the architecture of the Stewart–Gough platform. The actuator's lower and upper parts are fitted with universal joints Fig. 6(a). The actuated legs are mounted on the rings with eighteen especially patient-dedicated 3D-printed mounting parts (six 3D mounting parts on each ring), Fig. 6(b). This technical choice makes it possible to fix the ends of the six legs on elliptical curves around the patient-adapted rings.

2.2.2. The force sensors

Each actuator connects to a load cell (LCM200) to measure built for carrying inline tension or compression. The load cell used in this brace converts an input mechanical force such as tension and pressure into another physical variable, in this case, into an electrical output signal that is measured, transformed, and standardized. As the force applied to the load cell by the actuators increases, the electrical signal changes proportionally and helps to give information when the actuator exerts a force on the brace while parallel actuating. The linear actuators also feature an internal potentiometer for position feedback that can be input to an external controller. It has functionality for speed control, sensitivity control, stroke limits, and position control of the actuators. In addition, the position of the actuator's stroke length is driven with stable low and high reference voltage to read the position signal.

2.2.3. The motor drive

A motor driver (TB6612FNG) integrated a PWM control circuit with a 1000 Hz frequency into an electronic circuit. This PWM mode allows the control actuator to use a single digital output with the external controller of the brace. This mode of control with the motor driver varies the actuator speed so that it only consumes as much power as needed to drive the robotic brace without burning off the current as heat. It can also dissipate a power voltage supply of 15 V and 3.2 A of current, which is the required specification of the actuator. Also, it has a standby system (power save) that helps save power for the brace as the battery powers the whole mechanism.

2.2.4. The conditioning board

Each sensor interfaces with a conditioning board (ICA6H) capable of a 24 V high stability. These conditioning boards connect to the load cells to amplify the analog signals, convert them into digital format, and transfer them to the external controller of the brace. This conditioning board generates positive and negative supply rails, producing its standard 10 V output from a single 15–24 V supply equivalent to the actuator for better performance. Sensors are driven through it to get tension and compression of the actuator to determine the force exerted by the brace on the body.

2.3. Hardware and software configurations of the brace

A first 6 DOF parallel-actuated module is attached between the lower and middle ring, and a second one is between the middle and upper ring. Each module contains six actuators and two universal joints disposed at the extremities of the actuators. The actuators are driven at 12 V and 2 A employing a PWM signal of 1000 Hz; a built-in potentiometer in the actuator provides the position feedback of each actuator. The position feedback of each actuator is sent to the external controller. Each actuator integrates with a load cell on the underside of a part and conditioning that amplifies the load cell signals and sends them to the external controller of the brace to control the whole mechanism of the robotic brace. The actuator's position feedback and load cell voltage data are multiplexed and sent to the control board to drive the entire mechanism of the robotic brace. Position and force sensors can be used for control of every ring relative to the adjacent ring. With this architecture, the mid-thoracic ring can be controlled using the pelvic ring as a reference, either in force or position mode. Similarly, the thoracic ring can be controlled with respect to the thoracolumbar ring.

The system is portable and uses a controller programmed in Matlab and LabVIEW with custom-made electronic boards for real-time control of the motors and sensor communications.

A Lithium-polymer battery is the primary power source to run all the electronics. It can provide power to the system and continues to run all the mechanisms of the brace for up to 3–4 h with an output of 74 W of assistive force into the passive module.

3. Kinematics of the brace

3.1. Description of the mechanism of the platform

This section details the kinematic analysis of the Stewart–Gough platform, which is the fundamental principle of this designed robotic brace. Where Fig. 7 shows the architecture of the two parallel platforms. The kinematic structure of each leg is a UPU arrangement where linear electric actuators actuate prismatic links.

The actuators connect the fixed base to the moving platform at points $\mathbf{A}_i$ and $\mathbf{B}_i$, $i = 1, 2, \ldots, 6$. All the attachment points $\mathbf{A}_i$'s lie in the fixed base, and all the $\mathbf{B}_i$'s lie in the moving platform [36]. $\mathbf{O}_A$ and $\mathbf{O}_B$ are the center of the rings.

3.2. Mechanism models

We attached the fixed frame F_A to the base with center the point $\mathbf{O}_A$. Vectors $\boldsymbol{a}_i$ give the position of attachment points on the fixed base. Similarly, the moving frame F_B is attached to the moving platform with center the point $\mathbf{O}_B$, vectors give the position of moving attachment points $\boldsymbol{b}_i$'s. Its length $\boldsymbol{l}_i$ describes the geometrical parameter of each leg and unit vector $\boldsymbol{q}_i$ denotes its direction.

The vector $\mathbf{P_B} = [\mathbf{P}_{Bx}, \mathbf{P}_{By}, \mathbf{P}_{Bz}]^T$ describes the point $\mathbf{O}_B$ of the moving platform. The rotation matrix $\mathbf{R_B}$ describes the orientation of the moving platform [36, 37].

To analyze the inverse kinematic, we assume that the position $\mathbf{P_B}$ and orientation of the moving platform $\mathbf{R_B}$ are to get the joint variable of the legs (actuator), $\mathbf{L} = [l_1, l_2, \ldots, l_6]^T$.

(a)

(b)
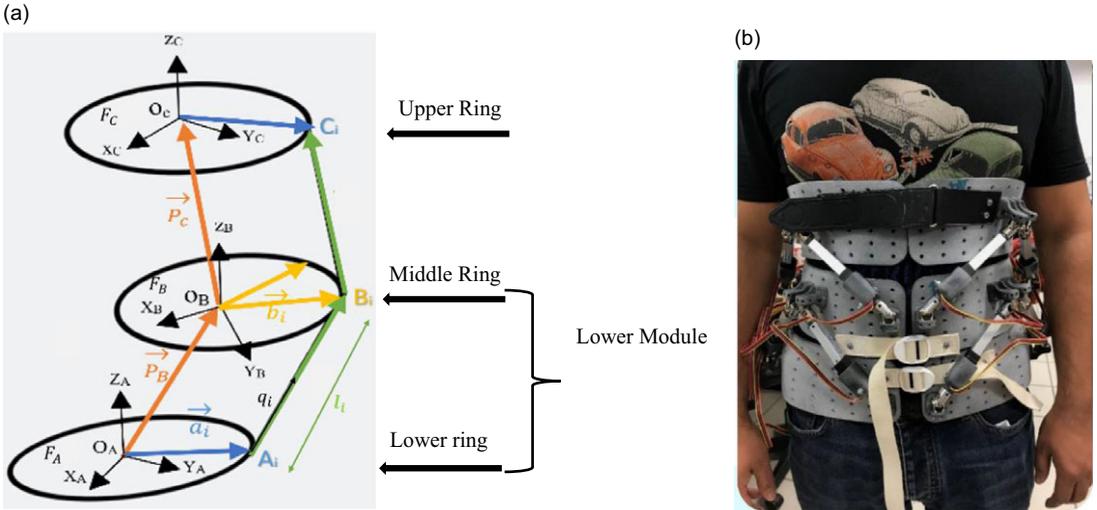
Figure 7. *(a) Schematics of the robotic brace, (b) Brace on volunteer.*

From the geometry as illustrated in Fig. 7(a), the closed-loop equation for each leg, $i = 1, 2, \ldots, 6$ is:

$$l_i q_i = -a_i + \mathbf{P_B} + b_i \tag{1}$$

The position of the origin $\mathbf{O_B}$ of frame B relative to frame A, where $\mathbf{R_B}$ is composed of three rotations from three angles (ψ_B, θ_B, ϕ_B).

$q = [q_1, q_2, \ldots, q_6]^T$ is the vector of the actuated joint variable of the leg (actuator) of the platform and $\mathbf{X_B} = [P_{Bx}, P_{By}, P_{Bz}, \psi_B, \theta_B, \phi_B]^T$ the vector of moving platform (second ring) motion variables [36, 37].

A shorthand notation is used for the equation below where (c) denotes cos and (s) denotes sin.

$$\mathbf{R_B} = \begin{bmatrix} c\theta_B.c\phi_B & s\psi_B.s\theta_B.c\phi_B - c\psi_B.s\phi_B & c\psi_B.s\theta_B.c\phi_B + s\psi_B.s\phi_B \\ c\theta_B.s\phi_B & s\psi_B.s\theta_B.s\phi_B + c\psi_B.c\phi_B & c\psi_B.s\theta_B.s\phi_B - s\psi_B.c\phi_B \\ -s\theta_B & s\psi_B.c\theta_B & c\psi_B.c\theta_B \end{bmatrix} \tag{2}$$

The legs $l_i\, q_i$ that connect the vertex points $\mathbf{A}_i$ and $\mathbf{B}_i$, for $i = 1, 2, \ldots, 6$ where these two Stewart platforms are similar, with the following constraints:

$$b_i = \mu a_i \quad \text{for } i = 1, \ldots, 6 \tag{3}$$

where μ is the constant of the scaling factor, so we have

$$a_i = a_{x_i}x + a_{y_i}y + a_{z_i}z \tag{4}$$

For Eq. (4) above its parameter, a_{xi}, a_{yi}, a_{zi} are the three components of a_i. And x, y, and z are three-unit vectors of frame A. Now using Eq. (1) for the closed loop, we have

$$l_i\, q_i = \mathbf{P_B} + \mathbf{R_B}.\, b_i - a_i$$

$$\mathbf{P_B} + (\mu\mathbf{R_B} - I)a_i \tag{5}$$

As written above for Eq. (5), in which $\mathbf{I}$ is an identity matrix, therefore, to calculate the lengths of the legs (actuators), we have here:

$$l_i^2 = q_i^T q_i + a_i^T[\mu\mathbf{R_B^T} - \mathbf{I})(\mu\mathbf{R} - \mathbf{I})]a_i + 2a_i^T(\mu\mathbf{R^T} - \mathbf{I})q_i \tag{6}$$

In forward kinematic analysis, we assumed that the leg lengths vector is given, and the problem is finding the position $\mathbf{P_B}$ and orientation of the moving platform $\mathbf{R_B}$. The problem depends on the representation used for orientation, where $\mathbf{X_B}$ is the computed screw axis representation of the rigid body.

An iterative numerical solver has been implemented in this study, and the "screw axis" method represents the rotation matrix. Detailed information about this method is available, particularly in [36–38].

$$\mathbf{X_B} = [\mathbf{P}_{Bx}, \mathbf{P}_{By}, \mathbf{P}_{Bz}, s_x, s_y, s_z, \mathbf{\Theta}]^T \tag{7}$$

where s_x, s_y, s_z, and $\mathbf{\Theta}$ are obtained by taking the difference between each pair of two opposing off-diagonal elements, which are given below as [36, 37]:

$$s_x = \frac{r_{32} - r_{23}}{2.\sin(\mathbf{\Theta})} \quad s_y = \frac{r_{13} - r_{31}}{2.\sin(\mathbf{\Theta})} \quad s_z = \frac{r_{21} - r_{12}}{2.\sin(\mathbf{\Theta})} \tag{8}$$

And the angle of rotation is obtained by summing the diagonal elements of the rotation matrix, which is given by:

$$\mathbf{\Theta} = \cos^{-1}\left(\frac{r_{11} + r_{22} + r_{33} - 1}{2}\right) \tag{9}$$

where r_{ij} represents the ith row and j^{th} column component of $\mathbf{R_B}$ for the computed $\mathbf{X_B}$. Pure rotation is through the screw axis of rotation $\hat{s}$ ($\hat{s}$ denotes unit vector) and an equivalent angle $\mathbf{\Theta}$ [36, 37]. The solution that can be used for the numerical iterative method is to compute the following seven nonlinear equations:

$$\mathbf{E}_i = -l_i^2 + \left[\mathbf{P_B} + \mathbf{R_B}.b_i - a_i\right]^T.[\mathbf{P_B} + \mathbf{R_B}.b_i - a_i] = 0 \quad \text{for } i = 1, \dots, 6$$
$$\mathbf{E}_7 = \hat{s}.\hat{s} = s_x^2 + s_y^2 + s_z^2 - 1 \tag{10}$$

The below equation is computed by numerical methods, which use nonlinear least-squares optimization routines [39], get a solution. In a least-squares problem, we minimize the function $\mathbf{E}(l_i)$ [40–42]. Finally, we consider the solution's iteration value calculated for minor square optimization with the accuracy $\in << 1$.

$$\mathbf{E}(l_i) = \frac{1}{2}\Sigma_i^7 \mathbf{E}_i \tag{11}$$

The Jacobian of the Stewart–Gough platform is given by the matrices, which are computed from closed-loop closures Eq. (1) to obtain:

$$\dot{\mathbf{P}}_B = \dot{q}_i - \omega_B.\mathbf{R_B}.b_i \quad \text{for } i = 1, \dots, 6 \tag{12}$$

in which angular velocity ω_B of the second ring relative to the first ring is [35, 37]:

$$\omega_B = \begin{bmatrix} \omega_1 \\ \omega_2 \\ \omega_3 \end{bmatrix} = \begin{bmatrix} 1 & 0 & -s\theta_B \\ 0 & c\psi_B & s\psi_B.c\theta_B \\ 0 & -s\psi_B & c\psi_B.c\theta_B \end{bmatrix} \begin{bmatrix} \dot{\psi}_B \\ \dot{\theta}_B \\ \dot{\phi}_B \end{bmatrix} \tag{13}$$

The twist of the ring as an input vector is defined as $\dot{\mathbf{X}}_B = [\dot{\mathbf{P}}_{Bx}, \dot{\mathbf{P}}_{By}, \dot{\mathbf{P}}_{Bz}, \omega_1, \omega_2, \omega_3]$ is mapped into the joint velocity vector of the moving platform by Jacobian as follows [36–38, 43].

Where b_i and q_i are the vector of the $\mathbf{P_B}$ and unit vector of the $\mathbf{A}_i\mathbf{B}_i$. To eliminate the ω_i with dot multiplication by q_i where six equations can be arranged in general formulation of the parallel Stewart–Gough platform kinematics, $(\mathbf{J}_x.\dot{\mathbf{X}} = \mathbf{J}_q.\dot{\mathbf{q}})$ can be rewritten as $\dot{q} = \mathbf{J}_q^{-1}.\mathbf{J}_X.\dot{\mathbf{X}}_B = \mathbf{J}.\dot{\mathbf{X}}_B$ with:

$$\mathbf{J} = \begin{bmatrix} \hat{q}_1^T & (b_1.\hat{q}_1)^T \\ \hat{q}_2^T & (b_2.\hat{q}_2)^T \\ \hat{q}_3^T & (b_3.\hat{q}_3)^T \\ \hat{q}_4^T & (b_4.\hat{q}_4)^T \\ \hat{q}_5^T & (b_5.\hat{q}_5)^T \\ \hat{q}_6^T & (b_6.\hat{q}_6)^T \end{bmatrix} \tag{14}$$

In our case, for the computed screw axis representation of the rotation matrix, q_i represents the unit vector which is the direction of the moving length of the leg (actuator). The below equation provides the transformation between the end effector output forces and the linear actuator forces. The vector assumption with the principle of virtual work is made that the leg applies a force only along the leg axis

$$\mathbf{F} = \mathbf{J}^T \boldsymbol{\tau}$$

$$
\begin{bmatrix}
F_x \\
F_y \\
F_z \\
M_x \\
M_y \\
M_z
\end{bmatrix}
=
\begin{bmatrix}
\hat{\boldsymbol{q}}_1 & \hat{\boldsymbol{q}}_2 \cdot \ldots \cdot \hat{\boldsymbol{q}}_6 \\
\boldsymbol{b}_1 \cdot \hat{\boldsymbol{q}}_1 & \boldsymbol{b}_2 \cdot \hat{\boldsymbol{q}}_2 \cdot \ldots \cdot \boldsymbol{b}_6 \cdot \hat{\boldsymbol{q}}_6
\end{bmatrix}
\cdot
\begin{bmatrix}
\tau_1 \\
\tau_2 \\
\tau_3 \\
\tau_4 \\
\tau_5 \\
\tau_6
\end{bmatrix}
\tag{15}
$$

in which $\boldsymbol{\tau} = [\tau_1, \tau_2, \ldots, \tau_6]^T$ is the vector of actuated joint torques or forces experienced by the legs (actuator force vector) and $\mathbf{F} = [F_x, F_y, F_z, M_x, M_y, M_z]^T$ represents vector of end effector output force and moment the end effector

3.3. The robotic brace trajectory

The trajectory of the brace is obtained with continuous acceleration, where different conditions are applied to position and velocity. The trajectory of the brace is assigned with necessary initial and desired and command values for the acceleration. Therefore, since there are six boundary conditions (position, velocity, and acceleration), a fifth-degree polynomial must be adopted, that is,

$$\mathbf{X}(t_0) = \mathbf{X}_0 \quad \dot{\mathbf{X}}(t_0) = \dot{\mathbf{X}}_0 \quad \ddot{\mathbf{X}}(t_0) = \ddot{\mathbf{X}}_0$$

$$\mathbf{X}(t_f) = \mathbf{X}_f \quad \dot{\mathbf{X}}(t_f) = \dot{\mathbf{X}}_f \quad \ddot{\mathbf{X}}(t_f) = \ddot{\mathbf{X}}_f$$

Trajectory planning is implemented for every DOF independently in the following manner [44]:

$$\mathbf{X}_i(t) = a_{0_i} + a_{1_i}t + a_{2_i}t^2 + a_{3_i}t^3 + a_{4_i}t^4 + a_{5_i}t^5 \tag{16}$$

The trajectory path implemented for the $\mathbf{X}(t)$ is a position vector. It gives the positions and orientations of the ring with respect to the other. We can have six equations in a matrix from the derivation of the initial and final constraints and their values [44].

$$
\begin{bmatrix}
1 & t_0 & t_0^2 & t_0^3 & t_0^4 & t_0^5 \\
1 & t_f & t_f^2 & t_0^3 & t_0^4 & t_0^5 \\
0 & 1 & 2t_0 & 3t_0^2 & 4t_0^3 & 5t_0^4 \\
0 & 1 & 2t_f & 3t_0^2 & 4t_0^3 & 5t_0^4 \\
0 & 0 & 2 & 6t_0 & 12t_0^2 & 20t_0^3 \\
0 & 0 & 2 & 6t_0 & 12t_0^2 & 20t_0^3
\end{bmatrix}
\cdot
\begin{bmatrix}
a_{0_i} \\
a_{1_i} \\
a_{2_i} \\
a_{3_i} \\
a_{4_i} \\
a_{5_i}
\end{bmatrix}
=
\begin{bmatrix}
\mathbf{X}_{0_i} \\
\mathbf{X}_{f_i} \\
\dot{\mathbf{X}}_{0_i} \\
\dot{\mathbf{X}}_{f_i} \\
\ddot{\mathbf{X}}_{0_i} \\
\ddot{\mathbf{X}}_{f_i}
\end{bmatrix}
\quad \textbf{for } \mathbf{i} = \mathbf{1}, \ldots, \mathbf{6} \tag{17}
$$

The determinant of the left-most matrix is $4(t_0 - t_f)^9$; thus; this matrix is invertible provided $t_0 \neq t_f$; therefore; the singular solution for the cubic polynomial coefficients can be determined [44].
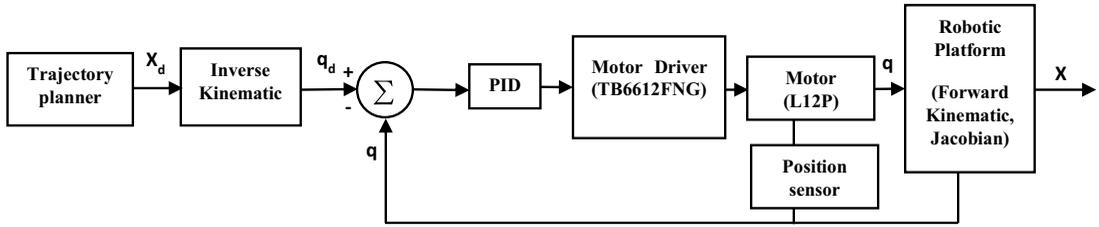
Figure 8. *Position controller implemented within the joint space.*

Furthermore, the cubic polynomial parameters can be simplified if the initial and desired motion velocities are equal to zero (rest), that is: $\dot{\mathbf{X}}_{0_i} = \dot{\mathbf{X}}_{f_i} = \ddot{\mathbf{X}}_{0_i} = \ddot{\mathbf{X}}_{f_i} = 0$ for $i = 1, \ldots, 6$ so that:

$$\mathbf{X}_i(t) = \mathbf{X}_{i0} - 10\left(\mathbf{X}_{i0} - \mathbf{X}_{if}\right)t^3 - 15\left(\mathbf{X}_{i0} - \mathbf{X}_{if}\right)t^4 - 6\left(\mathbf{X}_{i0} - \mathbf{X}_{if}\right)t^5$$

$$\dot{\mathbf{X}}_i(t) = -30(\mathbf{X}_{i0} - \mathbf{X}_{if})t^2 - 60(\mathbf{X}_{i0} - \mathbf{X}_{if})t^3 - 30(\mathbf{X}_{i0} - \mathbf{X}_{if})t^4$$

$$\ddot{\mathbf{X}}_i(t) = -60(\mathbf{X}_{i0} - \mathbf{X}_{if})t - 180(\mathbf{X}_{i0} - \mathbf{X}_{if})t^2 - 120(\mathbf{X}_{i0} - \mathbf{X}_{if})t^3 \tag{18}$$

The above trajectory will keep the brace resting at the initial and final motion.

4. Position control of the mechanism

We implemented position control in the joint space. Sensors attached to every leg give the controlled real-time joint position, enabling closed-loop control. The two Stewart–Gough platforms are controlled independently. They show the control topology for the position in Fig. 8, where a trajectory path generates to research the actuated platform motion. The controller then maps the required motions of the two platforms in Cartesian space $\mathbf{X}_d$ into the joint space variables (q_d) using inverse kinematics.

$\mathbf{X}_d = [\mathrm{P}_x, \mathrm{P}_y, \mathrm{P}_z, \psi, \theta, \phi]^{\mathrm{T}}$ is the vector of pose variables of the moving platform $\mathbf{X_B}$, and $q_d = [q_1, q_2, \ldots q_6]^{\mathrm{T}}$ is the vector of actuated joints [37, 43].

A part of the controller also computes the Cartesian position and force vectors, $\mathbf{X}$ of a platform, using the joint position feedback via forwarding kinematics and the robot's Jacobian. It enables the Cartesian applied force of a platform to be measured during position control [44]. The controller (an individual PID controller for every joint) receives the desired joint position q_d from the controller and performs the closed-loop control on the joint position. It measured the error as the difference between the specified and actual joint positions.

The actual position and orientation of the platform are obtained taking account the overall platform motions. The actual and desired leg lengths are then obtained, and leg positions are computed. To control the position, the obtained legs error are multiplied with the PID constant. For each actuator, we obtain the 3 control parameters of the PID via an experimental approach. The controller gains of every actuator based on the position are turned until errors were minor, and the system indicated better stability [33, 36, 45].

5. Controller evaluation

A range of time and motion study was performed by a healthy subject with the robot position controller. The brace origin center of each ring is calculated depending on the center of the circumference and analyzed together using motion analysis of the entire robotic brace. The x-axis is to the patient's left, the y-axis toward the anterior, and the z-axis vertically upwards for both parallel-actuated modules of the Stewart–Gough platform, see Fig. 9 (3D axis direction pitch-roll-yaw of the brace). Displacements and rotations (see Section 3) of the parallel-actuated platforms are relative to the corresponding axes of
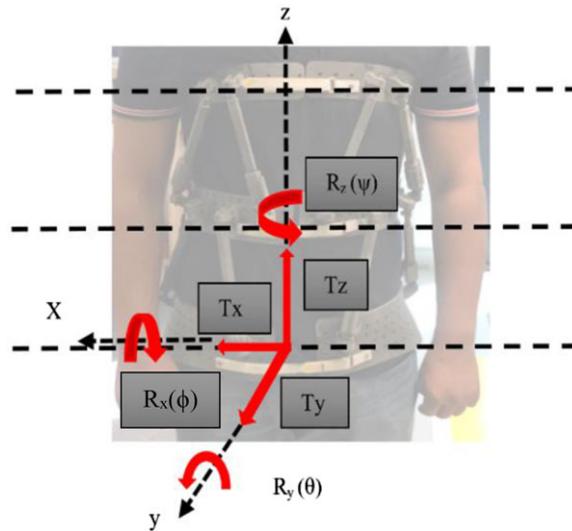
Figure 9. *The three axis of brace rotation.*

the respective rings within the neutral position and from the middle of the underside base frame of the rings.

5.1. Position controller validation

We evaluated the position controllers to determine the robot's performance regarding the actuator capabilities. In addition, we studied the system's range of motion to analyze the performance of the position control of the brace on a human subject.

We combined the Lower Body Marker set (LBM) without the foot (we use where eighteen markers in static configuration and sixteen in dynamic); see Fig. 10(b). The Upper Body Marker set is only around the spine and shoulders (with ten markers in static and dynamic); see Fig. 10(a). We use static markers while the motion capture system records the position of the markers on the brace. We then tracked the marker in space during motion, and then, the data were post-processed to define the position and motion of the brace relative to the body motion. During the data acquisition with the brace, spine markers had to reposition on the brace relative to anatomical landmarks. The position controller moved the brace through a range of translations and rotations.

Rotation around the z-axis and translation along the y-axis in the transverse plane was evaluated, denoted as three-point mode, as the traditional three-point correction in spine braces. In addition, we evaluated flexion and lateral bending to compare bending in the brace. We recorded the motion with the Qualisys® motion capture system. The translation and rotation of the middle and top rings are relative to the bottom base frame.

We used the markers highlighted in yellow in Fig. 10 for motion. The upper markers used for analysis are positioned on SJN-Sternum jugular notch, SXS-Sternum xiphisternal joint, CV7-7th cervical vertebrae, TV2-2nd thoracic vertebrae, MAI-the midpoint between inferior angles of most caudal points of the scapulae, LV1, LV3, LV5 (1st, 3rd and 5th lumbar vertebrae), L_SAE- and R_SAE (scapula acromial edge) for the UBM sets. The LBM sets are used for static and dynamic data acquisition.

The lower markers used for analysis are positioned on the L_FCC-Aspect of the Achilles tendon insertion on the calcaneus, L_FM1-Dorsal margin of the first metatarsal head, L_FM2-Dorsal margin of the second metatarsal head, L_FM5-Dorsal margin of the fifth metatarsal head, R_FCC- Aspect of the Achilles tendon insertion on the calcaneus, R_FM1-Dorsal margin of the first metatarsal head, R_FM2-Dorsal margin of the second metatarsal head, R_FM5-Dorsal margin of the fifth metatarsal head. Once
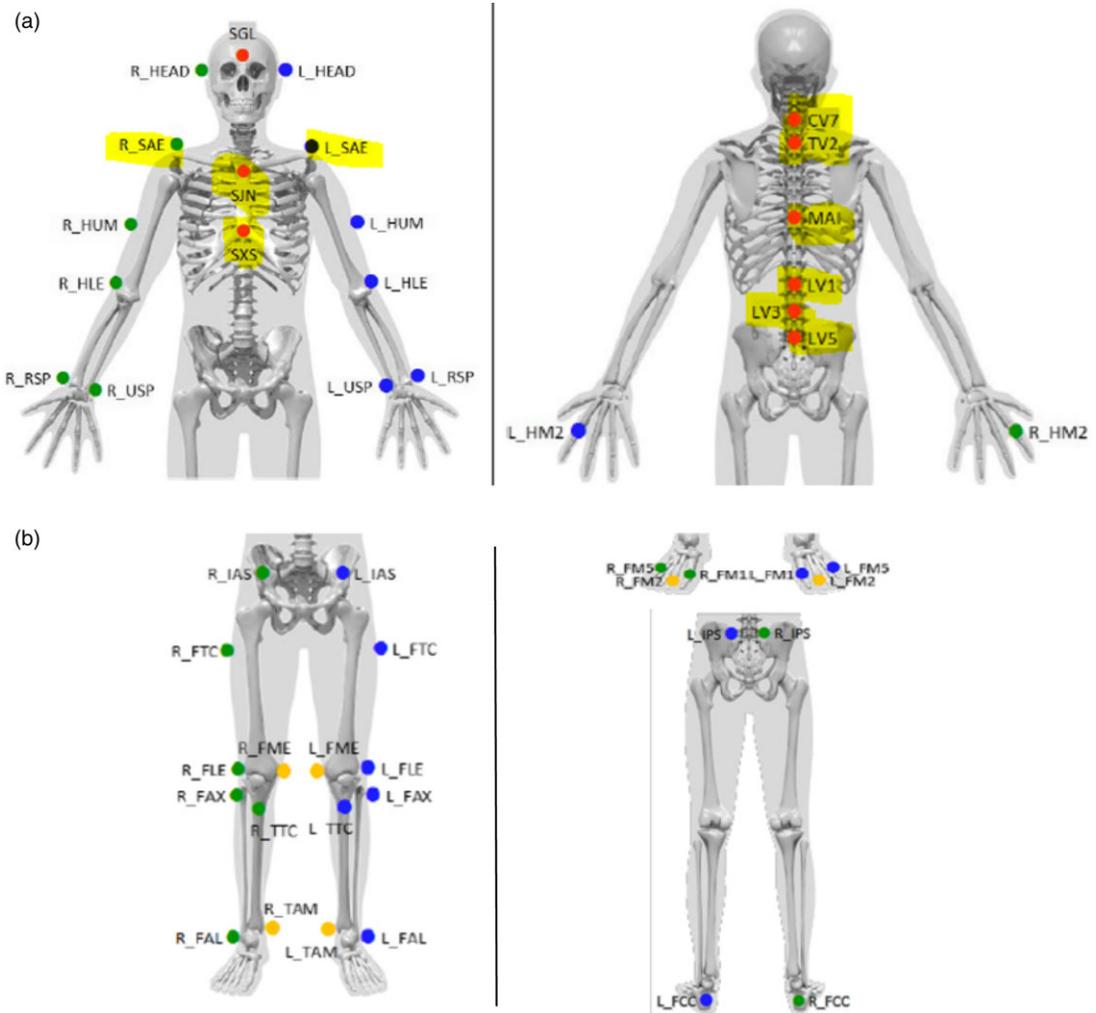
Figure 10. *Motion analysis marker set: (a) position on the upper body; (b) position on the lower body.*

we do the data and information acquisition on the brace, we have markers for each ring. It is essential for 3D reconstruction on visual 3D and analysis of the motion imposed by the brace.

For each ring, we place four markers, see Fig. 11. Three are used to define the plane characterizing the ring position (markers BL1 to BL3 are associated with the lower ring, BM1-BM3 for the middle ring, and BU1-BU3 for the upper ring).

A theoretical brace center is defined, point O, represented in blue in Fig. 11, between BL1 and BL3. The line between point O and the center of BL1 and BL3 (in blue) gives the X-axis; the Z-axis is orthogonal to the plane.

5.2. Experimental evaluation of robot position

The linear actuator in each leg has an integrated potentiometer that feeds back the joint displacement from which we compute the Cartesian pose of every ring using forward kinematics. In addition, we placed infrared markers on the rings to measure their position and orientation with a motion capture system.
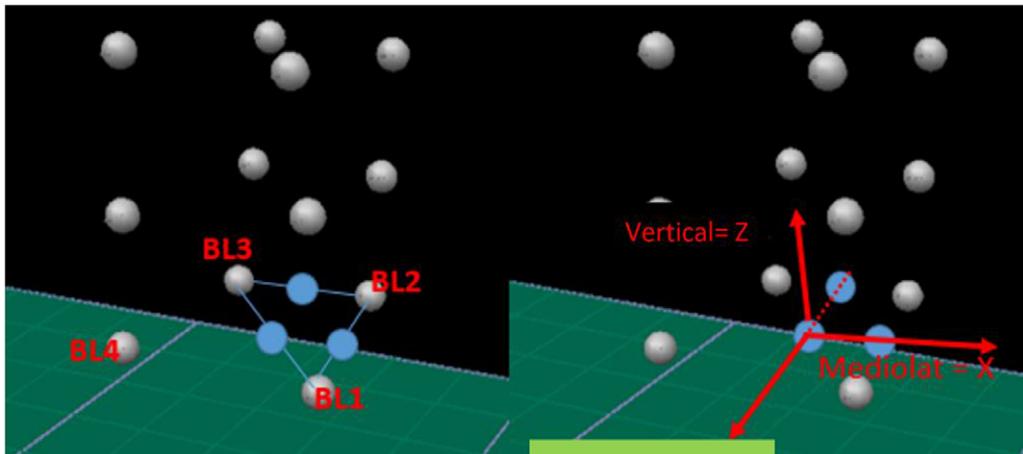
Figure 11. *Motion analysis* 3D *construction with marker positions.*

The robot position is evaluated by moving the brace through different modes of motion:

(1) Torso flexion, (2) lateral bending, (3) rotation following, (4) rotation mirroring, (5) translation following, and (6) translation mirroring.

We evaluated all the modes taking the three-point pressure principle into account.

Based on human biomechanics, the three-point pressure mode is the general principle used to correct abnormal spine curves in braces. This mode of spinal correction may involve rotation around the z-axis and translation along the y-axis through the transverse plane. In addition, sagittal trunk flexion and frontal bending modes evaluate the bending motion capability of the brace.

We applied the series of modes for isolated translations and rotations. In these modes, the robotic brace's upper parallel module (middle ring articulated with upper ring) performed the identical task (following). The lower parallel module (lower ring articulated with middle ring) of the brace performs the alternative task (mirroring); see Fig. 7(b).

We recorded the motion using a motion capture system and a potentiometer providing position feedback of the actuator while being attached to the underside of this actuator. The translation's interpretation and rotation of the middle and top ring are relative to the position and analyzed concerning the lower ring coordinate frame of the robotic brace. Figure 12 shows motion tracking results verified using a motion capture system for a three-point-pressure motion trial. The robot position controller could follow all paths for all tested trajectories. We calculate the position and rotation of the middle and upper ring relative to the lower ring coordinate frame see Fig. 12.

We can observe that the middle ring has more noteworthy rotations than the upper one. Therefore, for the prosthesis, it is necessary to have greater mobility of the middle ring than the upper, so the brace model correctly follows the patient's movement. We conducted other tests with or without a brace to compare the amplitude of the patient's movements [26, 37]. We will perform future experiments with patients with scoliosis to confirm the performances of the brace in a real medical case.

6. The robotic brace for improved patient interaction

The current prototype of the robotic brace is not as low profile as currently used braces made of rigid plastic sheets. For the patient's comfort, we designed it with a low weight (2.5 kg) compared to other active braces taken into consideration in the literature presented above. It can realize precise control over the vertebra by continuously applying force on the spine and is fabricated quickly with the exact working mechanism regardless of the body structure of the users. We modulate it based on the user's needs, follow the body motion simultaneously, and do not limit daily activities, including eating, sitting, standing, and other sporting activities. As a result, it will prevent pain, muscle breakdown, and abnormal
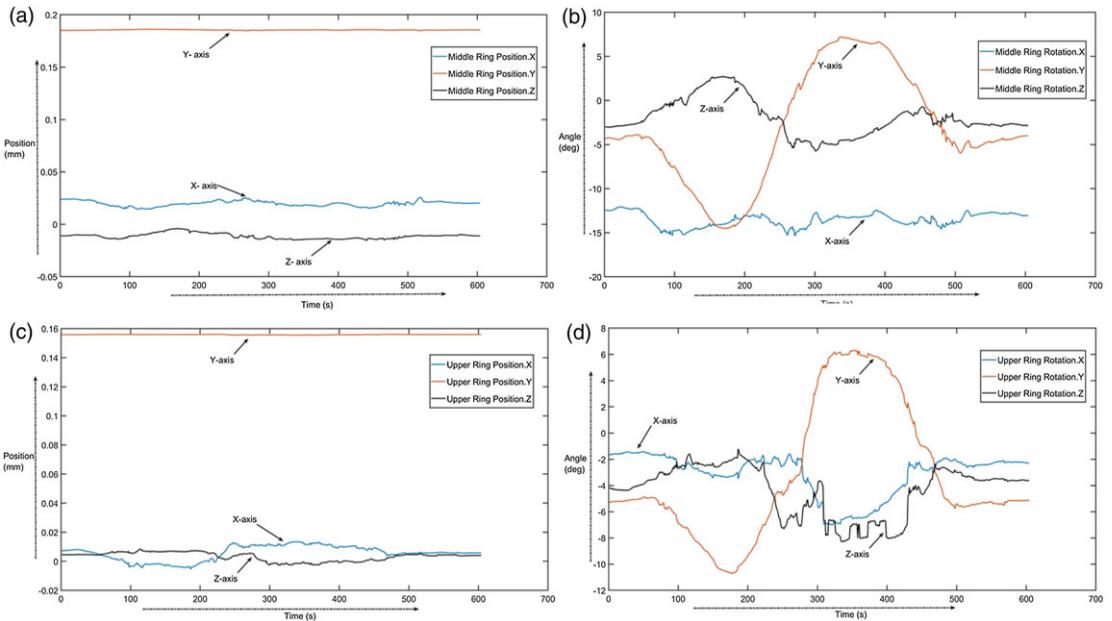
Figure 12. *Graphical representation of the Qualisys motion capture results from the three-point mode test. Rotation and translation about x, y, and z are represented by blue, red, and black, respectively. (a) Position of the Middle ring origins; (b) Rotation angles of the middle ring; (c) Position of the upper ring (d) Rotation angles of the upper ring.*

deformation of bone. However, compliance with the bracing technique continues to be a hurdle as many patients who suffer from an abnormal Spine posture observe the prescribed 12–16 h of daily wear.

Control strategies reduce the time patients must wear the brace while continuing to treat the abnormal curves of the spine with no adverse impact. Suppose the wearer can receive the identical quality of care while only wearing the brace for 6 h a day. In that case, compliance may increase, and individuals may be more likely to benefit from bracing. Hasler et al. have shown [46] that flexible bracing does not improve compliance if it still requires long-duration wear. The robotic brace presented here is one of a kind. It can hopefully facilitate the way for a new approach in bracing methods to treat scoliosis and other spine deformity problems. Improvements still need to be made to the current robotic brace, and the next steps will be to better match the clinical process and materials for fabricating the brace frame. It is also necessary to improve the design and make it lighter for better comfort. A more compact control board and other electronic designs could make the system portable and easier to wear. We will integrate more sensors into the brace to measure the precise force exerted on the body and vice versa. It will help monitor the body's applied force by the brace to improve the excessive pressure on the body. We will add position sensors for better orientation to compute the kinematics of the brace and capture the patient's intention for the motion adaption. Further medical tests will be performed, and we should retrieve patient opinions to evaluate the effectiveness and comfort of the robotic brace and compare it to traditional bracing techniques. We will also use the brace for lab studies for spinal correction as a part of future evaluations.

7. Conclusion

This paper has presented a robotic brace for scoliosis patients. We designed it to enhance the patient's quality of life. Because scoliosis is a complex three-dimensional deformity, it is necessary to apply three-dimensional controllable corrective three-point pressure on the human spine to correct the deformation

fully. The motivation for this work comes from the limitation of current bracing methods. Our goal was to design a comfortable brace that has controllable motions and pressure. It is composed of two modules with Stewart–Gough platforms in series. Each platform is independently controlled in motion or position. It allows continuous exertion of three-point pressure on the human body and simultaneously allows the patient's usual movements (sagittal and frontal flexions, axial rotation). First, from a scanner, we optimized the overall shapes of the designed prototype to fit on the human torso. A rapid prototyping technique was used to produce the devices. Finally, we performed motion tests in a prosthesis company on a healthy human to validate the brace kinematic architecture choice and its control strategies: position and motion control. As such, a robotic brace needs to be designed particularly for each patient, and the range of motions depends on the severity of the disease, and it is necessary to perform new experiments with different persons (adults and adolescents) and different pathology levels to completely validate the design.

References

[1] A. A. De Smet, M. A. A. L. T. Cook, J. E. Goin, H. G. Scheuch and J. M. Orrick, "Three-dimensional analysis of right thoracic idiopathic scoliosis," *Spine* **9**(4), 377–381 (1984).

[2] I. Stokes, L. Bigalow and M. Moreland, "Three-dimensional spinal curvature in idiopathic scoliosis," *J. Orthop. Res.* **5**(1), 102–113 (1987).

[3] J. W. Roach, "Adolescent idiopathic scoliosis," *Orthop. Clin. North Am.* **30**(3), 353–365 (1999).

[4] B. V. Reamy and J. B. Slakey, "Adolescent idiopathic scoliosis: Review and current concepts," *Am. Fam. Phys.* **64**(1), 111 (2001).

[5] S. Weinstein, L. Dolan, J. Wright and M. Dobbs, "Effects of bracing in adolescents with idiopathic scoliosis," *Child Care Health Develop.* **40**(1), 146–147 (2014).

[6] S. Weinstein, L. Dolan and J. Wright, "Design of the bracing in adolescent idiopathic scoliosis trail (BrAIST)," *Spine* **38**(21), 1832–1841 (2013).

[7] C. Yang, B. Tian, X. Li, S. Zheng and S. K. Agrawal, "Investigation of robotic braces of patients with idiopathic scoliosis," *J. Mech. Med. Biol.* **18**(08), 8 (2018).

[8] J. Cheng, R. Castelein, W. Chu, A. Danielsson, M. Dobbs, T. Grivas, C. Gurnett, K. Luk, A. Moreau, P. Newton, I. Stokes, S. Weinstein and R. Burwell, "Adolescent idiopathic scoliosis," *Nat. Rev. Dis. Primers* 1, 15030 (2015).

[9] S. Weinstein and I. Ponseti, "Curve progression in idiopathic scoliosis," *J. Bone Joint Surg.* **65**(4), 447–455 (1983).

[10] J. Lonstein and R. Winter, "The Milwaukee brace for the treatment of adolescents idiopathic scoliosis. A review of one thousand and twenty patients," *J. Bone Joint Surg.* **76**(8), 1207–1221 (1994).

[11] D. Skaggs, "Effectiveness of treatment with a brace in girl who have adolescent idiopathic scoliosis. A prospective controlled study based on data from the brace study of the scoliosis research society," *J. Bone Joint Surg.* **78**(1), 151 (1996).

[12] C. Nnadi and J. Fairback, "Scoliosis: A review," *Pediatr. Child Health* **20**(5), 215–220 (2009).

[13] J. Carlson, "Clinical biomechanics of orthotic treatment of idiopathic scoliosis," *J. Prosthet. Orthot.* **15**(4S), 17–S30 (2003).

[14] R. Heary, C. Bono and S. Kumar, "Bracing for scoliosis," *Neurosurgery* **63**(3), A125–A130 (2008).

[15] S. Negrini and S. Minozzi. *Braces for Idiopathic Scoliosis in Adolescents* (John Wiley & Sons, New York, NY, 2010).

[16] S. Weinstein, L. Dolan, J. Wright and M. Dobbs, "Effects of bracing in adolescents with idiopathic scoliosis," *N. Engl. J. Med.* **369**(16), 1512–1521 (2013).

[17] J. Wynne, "The boston brace system philosophy, biomechanics, design & fit," *Stud. Health Technol. Inform.* **135**(1), 370–384 (2007).

[18] M. Rigo and H. Weiss, "The cheneau concept of bracing - biomechanical aspects," *Stud. Health Technol. Inform.* **135**(1), 303–319 (2008).

[19] C. Price, D. Scott, F. Reed and M. Riddick, "Night-time bracing for adolescent idiopathic scoliosis with the charleston bending brace: Preliminary report," *Spine* **15**(12), 1294–1299 (1990).

[20] J. Lonstein and R. Winter, "Milwaukee brace for the treatment of adolescent idiopathic scoliosis: A review of one thousand and twenty patients," *J. Bone Joint Surg.* **76**(8), 1207–1221 (1994).

[21] D. Federico and T. Renshaw, "Results of treatment of idiopathic scoliosis with the Charleston bending orthosis," *Spine* **15**(9), 886–887 (1990).

[22] W. Blount, "The milwaukee brace in the treatment of the young child with scoliosis," *Arch. Orthop. Traum Surg.* **56**(4), 363–369 (1964).

[23] H. Watts, J. Hall and W. Stanish, "The Boston brace system for the treatment of low thoracic and lumbar scoliosis by the use of girdle without superstructure," *Clin. Orthop. Relat. Res.* **126**(126), 87–92 (1977).

[24] H. Labelle, J. Dansereau, C. Bellefleur and B. Poitras, "Three-dimensional effect of the Boston brace on the thoracic spine and rib cage," *Spine* **21**(1), 59–64 (1996).

[25] H. Weiss and M. Rigo, "The cheneau concept of bracing - actual standards," *Stud. Health Technol. Inform.* **135**(1), 291–302 (2008).

[26] J. Mac-Thiong, Y. Petit, C. Aubin, S. Delorme, J. Dansereau and H. Labelle, "Biomechanical evaluation of the boston brace system for the treatment of adolescent idiopathic scoliosis: Relationship between strap tension and brace interface forces," *Spine* **29**(1), 26–32 (2004).

[27] C. Aubin, H. Labelle, A. Ruszkowsk, Y. Petit, D. Gignac, J. Joncas and J. Dansereau, "Variability of strap tension in brace treatment for adolescent idiopathic scoliosis," *Spine* **24**(4), 349–354 (1993).

[28] M. Wong, J. Cheng, T. Lam, N. G. B., S. Sin, S. Lee-Shum, D. Chow and S. Tam, "The effect of rigid versus flexible spinal orthosis on the clinical efficacy and acceptance for the patients with adolescent idiopathic scoliosis," *Spine* **33**(12), 1360–1365 (2008).

[29] C. Coillard, V. Vachon, A. Circo, M. Beausejour and C. Rivard, "Effectiveness of the spinecor brace based on the new standardized criteria proposed by the scoliosis research society for adolescent idiopathic scoliosis," *J. Pediatr. Orthoped.* **27**(4), 375–379 (2007).

[30] E. Lou, S. Venkateswaran, D. Hill, J. Raso and A. Donauer, "An intelligent active brace system for the treatment of scoliosis," *IEEE Trans. Instrum. Meas.* **53**(4), 1146–1151 (2004).

[31] "ExMS-1," ExoDynamics, LLC, [Online]. Available: www.exodynamicsmedical.com [Accessed 23/04/2019].

[32] J. Park, P. R. Stegall, D. P. Roye and S. K. Agrawal, "Robotic spine exoskeleton (RoSE): Characterizing the 3-d stiffness of the human torso in the treatment of spine deformity," *IEEE Trans. Neural Syst. Rehabil. Eng.* **26**(5), 1026–1035 (2018).

[33] R. Ray, L. Nouaille, B. Colobert and Poisson G., "Design of Robotic Braces for Patients with Scoliosis," **In**: *RAAD 2020*, Mechanism and Machine Science, vol. 84 (Springer, Cham, 2020) pp. 1–8.

[34] J. Merlet, "Direct kinematics of parallel manipulators," *IEEE Trans. Robot. Autom.* **9**(6), 842–845 (1993).

[35] K. Waldron and K. Hunt, "Series-parallel dualities in actively coordinated mechanisms," *Int. J. Robot. Res.* **10**(5), 473–480 (1991).

[36] L. W. Tasi, *Robot Analysis* (John Wiley & Sons, Inc., New York, NY, 1999).

[37] H. Taghirad, *Parallel Robots* (CRC Press, Boca Raton, FL, 2012).

[38] J. Park, P. Stegall and S. K. Agrawal, "Dynamic Brace for Correction of Abnormal Postures of the Human Spine," **In**: *Proceedings of the IEEE International Conference on Robotics and Automation, Seattle, WA* (2015) pp. 5922–5927.

[39] J. J. Moré, *Numerical Analysis*, Lecture Notes in Mathematics (Springer, Berlin, 1977) pp. 405–116.

[40] J. E. Dennis and R. B. Schnabel, *Numerical Methods for Unconstrained Optimization and Nonlinear Equations*, Prentice-Hall Series in Computational Mathematics (Prentice-Hall, Englewood Cliffs, NJ, 1983).

[41] K. Levenberg, "A method for the solution of certain problems in least-squares," *Q. Appl. Math.* **2**(2), 164–168 (1944).

[42] D. Marquardt, "An algorithm for least-squares estimation of nonlinear parameters," *SIAM J. Appl. Math.* **11**(2), 431–441 (1963).

[43] L. Biagiotti and C. Melchiorri, *Trajectory Planning for Automatic Machines and Robots* (Springer, Cham, 2008).

[44] C. Gosselin, "Stiffness mapping of parallel manipulators," *IEEE Trans. Robot. Autom.* **6**(3), 377–382 (1990).

[45] R. Ray, L. Nouaille, B. Colobert, L. Calistri and G. Poisson, "Design of a Robotic Brace with Parallel Structure for Spine Deformities Correction," **In**: *MEDER 2021: Mechanism Design for Robotics*, vol. 103 (Springer, Cham, 2021) pp. 159–167.

[46] C. C. Hasler, S. Wietlisbach and P. Buchler, "Objective compliance of adolescent girls with idiopathic scoliosis in a dynamic spinecor brace," *J. Child. Orthop.* **4**(3), 211–218 (2010).